

An unbiased method of measuring the ratio of two data sets

ZEYANG SUN ^{1,2,*} PENGJIE ZHANG,^{1,2,3,†} FUYU DONG ⁴, JI YAO ⁵, HUANYUAN SHAN ^{5,6}, ERIC JULLO ⁷,
JEAN-PAUL KNEIB,^{7,8} AND BOYAN YIN⁹

¹*Department of Astronomy, School of Physics and Astronomy, Shanghai Jiao Tong University, Shanghai, 200240, China*

²*Key Laboratory for Particle Astrophysics and Cosmology (MOE) / Shanghai Key Laboratory for Particle Physics and Cosmology, China*

³*Division of Astronomy and Astrophysics, Tsung-Dao Lee Institute, Shanghai Jiao Tong University, Shanghai, 200240, China*

⁴*South-Western Institute for Astronomy Research, Yunnan University, Kunming, 650500, China*

⁵*Shanghai Astronomical Observatory (SHAO), Nandan Road 80, Shanghai, 200030, China*

⁶*University of Chinese Academy of Sciences, Beijing, 100049, China*

⁷*Aix-Marseille Univ, CNRS, CNES, LAM, Marseille, France*

⁸*Institute of Physics, Laboratory of Astrophysics, Ecole Polytechnique Fédérale de Lausanne (EPFL), Observatoire de Sauverny, 1290 Versoix, Switzerland*

⁹*Department of Physics, Carnegie Mellon University, Pittsburgh, Pennsylvania 15312, USA*

ABSTRACT

In certain cases of astronomical data analysis, the meaningful physical quantity to extract is the ratio R between two data sets. Examples include the lensing ratio, the interloper rate in spectroscopic redshift samples, the decay rate of gravitational potential and E_G to test gravity. However, simply taking the ratio of the two data sets is biased, since it renders (even statistical) errors in the denominator into systematic errors in R . Furthermore, it is not optimal in minimizing statistical errors of R . Based on Bayesian analysis and the usual assumption of Gaussian error in the data, we derive an analytical expression of the posterior PDF $P(R)$. This result enables fast and unbiased R measurement, with minimal statistical errors. Furthermore, it relies on no underlying model other than the proportionality relation between the two data sets. Even more generally, it applies to the cases where the proportionality relation holds for the underlying physics/statistics instead of the two data sets directly. It also applies to the case of multiple ratios ($R \rightarrow \mathbf{R} = (R_1, R_2, \dots)$). We take the lensing ratio as an example to demonstrate our method. We take lenses as DESI imaging survey galaxies, and sources as DECaLS cosmic shear and *Planck* CMB lensing. We restrict the analysis to the ratio between CMB lensing and cosmic shear. The resulting $P(R)$, for multiple lens-shear pairs, are all nearly Gaussian. The S/N of measured R ranges from 4.9 to 8.4. We perform several tests to verify the robustness of the above result.

Keywords: gravitational lensing: weak — methods: statistical — large-scale structure of Universe — cosmology: observations — cosmic background radiation

1. INTRODUCTION

In astronomy data analysis (e.g. cosmological analysis), we often need to combine different data sets for joint analysis. In certain cases, the desirable quantity to extract from the joint data is the ratio of two data sets. We list several examples as follows. (1) The lensing ratio (Jain & Taylor 2003; Bernstein & Jain 2004; Zhang et al. 2005). This is the ratio of galaxy-galaxy lensing of different sources (e.g. cosmic shear at various redshifts

and CMB lensing) but identical lenses. The ratio provides a clean measure on the geometry of the universe. It has been measured for various data combinations (Taylor et al. 2007; Das & Spergel 2009; Kitching et al. 2015; Baxter et al. 2016; Miyatake et al. 2017; Prat et al. 2018, 2019; Omori et al. 2019; Sánchez et al. 2021). (2) The decay rate DR of gravitational potential, which is the ratio between galaxy-ISW cross-correlation and galaxy-lensing cross-correlation (Zhang 2006). It has recently been measured by Dong et al. (2022) combining DESI galaxy-Planck ISW/lensing cross-correlations. The DR measurement, in combination with BAO or SNe Ia data, improved constraints of dark energy by $\sim 20\text{-}50\%$ (Dong

* zeyangsun@sjtu.edu.cn

† zhangpj@sjtu.edu.cn

et al. 2022). (3) Interloper rate due to line confusion in spectroscopic redshift surveys. This particular error in redshift measurement can be approximated as the ratio between the cross-correlation of two target galaxy samples and the auto-correlation (e.g. Addison et al. (2019); Farrow et al. (2021); Gong et al. (2021)). (4) E_G as a probe of gravity at cosmological scales (Zhang et al. 2007). It is essentially the ratio between cross-correlations of galaxy-velocity and galaxy-lensing. It has been measured by Reyes et al. (2010); Leonard et al. (2015); Blake et al. (2016); Pullen et al. (2016); Alam et al. (2017); de la Torre et al. (2017); Amon et al. (2018); Singh et al. (2019); Skara & Perivolaropoulos (2020); Zhang et al. (2021a), using various data of redshift space distortion (RSD) and weak lensing.

The ratio is therefore straightforward to measure by simply taking the ratio of the two corresponding measurements. However, there are a number of reasons to improve this naive estimator. (1) The naive estimator is not only sub-optimal in terms of statistical errors, but also biased. Suppose that we have two data sets, $D_1 = \bar{D}_1(1 + n_1)$ and $D_2 = \bar{D}_2(1 + n_2)$. Here \bar{D} is the true value the theory predicts $\bar{D}_2/\bar{D}_1 = R$. n is the fractional error and for brevity we assume only statistical error here ($\langle n \rangle = 0$). The naive estimator $\hat{R} = D_2/D_1$ is biased since

$$\langle \hat{R} \rangle = \left\langle \frac{D_2}{D_1} \right\rangle = R (1 + \langle n_1^2 \rangle - \langle n_1 n_2 \rangle + \dots) \neq R. \quad (1)$$

(2) Furthermore, in some applications the physically meaningful R is not directly the ratio of two data sets, but rather the ratio of some underlying models. For example, one data set is the galaxy-tangential shear cross-correlation, and the other is the galaxy-CMB lensing convergence cross-correlation. The first is related to the galaxy-lensing power spectrum through the Bessel function $J_2(x = \ell\theta)$. The second is related to $J_0(x)$ instead. So although the underlying galaxy-lensing power spectra follow the proportionality relation, the data sets do not. Another example is E_G , as measured by combining a 3D galaxy-velocity power spectrum inferred from RSD and a 2D galaxy-lensing angular power spectrum. In both cases, we can not simply take the ratio of two data sets to obtain the true ratio. (3) A further issue is that there are multiple R of interest (namely $\mathbf{R} = (R_1, R_2, \dots)$), but the corresponding data sets to measure them are correlated. This is the case for the interloper rate, and also the more general case of photo- z outliers.

We present a likelihood-based optimal estimator of the ratio, free of the above problems. Under the usual assumption of Gaussian errors in the data, we derive the exact analytical expression for the posterior PDF $P(R)$

(or the joint PDF $P(\mathbf{R}) = P(R_1, R_2, \dots)$). Since the expression is exact, it enables unbiased R estimation with minimum statistical uncertainty. The method has been applied in a companion paper (Dong et al. 2022) to measure the decay rate of gravitational potential at cosmological scales. Here we present a thorough description of the method, and further demonstrate its applicability with the lensing ratio measurement as an example.

The paper is organized as follows. In §2, we introduce the method. In §3, we show the application of this method by measuring lensing ratios, including the measurements of the lensing ratios (§3.1) and the consistency checks (§3.2). We conclude in §4. Appendix A describes the data pre-processing. Appendix B shows the details on the lensing ratio statistics, ratio modeling, and implications of the measured ratio.

2. METHODOLOGY

The problem to be solved can be formulated as follows. We have two data sets, \mathbf{d}_1 and \mathbf{d}_2 . The theory expectation of \mathbf{d}_1 is fixed by the theory parameter vector $\boldsymbol{\lambda}$, $\mathbf{d}_1 = \mathbf{A}_1 \boldsymbol{\lambda} + \mathbf{n}_1$. Here the mapping matrix \mathbf{A}_1 of dimension $N_{\mathbf{d}} \times N_{\boldsymbol{\lambda}}$. \mathbf{n}_1 is the corresponding noise, which we assume to be Gaussian with zero mean. \mathbf{d}_2 is fixed by the same set of theory parameter $\boldsymbol{\lambda}$ and an extra parameter R . The dependence on R is through the second mapping matrix $\mathbf{A}_2(R)$, $\mathbf{d}_2 = \mathbf{A}_2(R) \boldsymbol{\lambda} + \mathbf{n}_2$. The simplest case is $\mathbf{A}_2 = R \mathbf{A}_1$. This is the case for the shear ratio, where $d_i = w_i(\theta)$, $\boldsymbol{\lambda} = \langle w_1(\theta) \rangle$, and $w_i(\theta)$ are the two galaxy-shear cross-correlations. But in general A_2 and A_1 are independent, and $\mathbf{A}_2(R)$ can be an arbitrary function of R or even $\mathbf{R} = (R_1, R_2, \dots)$. For brevity, we work on the case of R . The extension to the more general case of \mathbf{R} is straightforward.

We can study this problem based on Bayesian analysis,

$$P(R|\mathbf{d}_1, \mathbf{d}_2) \propto \int P(\mathbf{d}_1, \mathbf{d}_2|R, \boldsymbol{\lambda}) P(\boldsymbol{\lambda}) P_{\text{prior}}(R) d\boldsymbol{\lambda}. \quad (2)$$

We take a flat prior of $\boldsymbol{\lambda}$ ($P(\boldsymbol{\lambda}) \propto \text{const.}$) in order not to introduce extra model dependence. $P_{\text{prior}}(R)$ refers to the prior of R , and we explain its choice at the end of this section. What we find is that, for Gaussian distribution of the data, the marginalization over $\boldsymbol{\lambda}$ can be done analytically. So we can obtain an analytical expression of $P(R)$. The expression depends on whether $\mathbf{d}_{1,2}$ are correlated. We first derive the result for the simpler case of uncorrelated $\mathbf{d}_{1,2}$, and then proceed to the general case of correlated $\mathbf{d}_{1,2}$.

2.1. Uncorrelated $\mathbf{d}_{1,2}$

When measurement errors in $\mathbf{d}_1, \mathbf{d}_2$ are uncorrelated, the joint likelihood on the right-hand-side of Eq. 2 can be

separated into the product of two individual likelihood functions,

$$P(\mathbf{d}_1, \mathbf{d}_2 | R, \boldsymbol{\lambda}) = P(\mathbf{d}_1 | R, \boldsymbol{\lambda}) P(\mathbf{d}_2 | R, \boldsymbol{\lambda}) . \quad (3)$$

For Gaussian distributed $\mathbf{d}_{1,2}$,

$$P(\mathbf{d}_i | R, \boldsymbol{\lambda}) = \frac{1}{\sqrt{(2\pi)^N \det \mathbf{C}_i}} \exp \left[-\frac{1}{2} \boldsymbol{\Delta}_i^T \mathbf{C}_i^{-1} \boldsymbol{\Delta}_i \right] .$$

Here $\boldsymbol{\Delta}_i \equiv \mathbf{d}_i - \mathbf{A}_i \boldsymbol{\lambda}$. \mathbf{C}_i is the covariance matrix of \mathbf{d}_i , $\mathbf{C}_i \equiv \langle \mathbf{n}_i \mathbf{n}_i^T \rangle$. All vectors are column vectors by default, like $\boldsymbol{\lambda}^T = (\lambda_1, \lambda_2, \dots, \lambda_N)$. N is the size of $\mathbf{d}_{1,2}$. Plugging the above expression into Eq. 2 & 3,

$$P(R | \mathbf{d}_1, \mathbf{d}_2) \propto \int \exp(E) P_{\text{prior}}(R) d\boldsymbol{\lambda} . \quad (4)$$

We have to ignore the proportionality prefactors which do not depend on $\boldsymbol{\lambda}$. E in the exponential is

$$\begin{aligned} E = & -\frac{1}{2} (\boldsymbol{\lambda}^T \mathbf{A}_1^T \mathbf{C}_1^{-1} \mathbf{A}_1 \boldsymbol{\lambda} - \boldsymbol{\lambda}^T \mathbf{A}_1^T \mathbf{C}_1^{-1} \mathbf{d}_1 - \mathbf{d}_1^T \mathbf{C}_1^{-1} \mathbf{A}_1 \boldsymbol{\lambda} \\ & + \mathbf{d}_1^T \mathbf{C}_1^{-1} \mathbf{d}_1 + \boldsymbol{\lambda}^T \mathbf{A}_2^T \mathbf{C}_2^{-1} \mathbf{A}_2 \boldsymbol{\lambda} - \boldsymbol{\lambda}^T \mathbf{A}_2^T \mathbf{C}_2^{-1} \mathbf{d}_2 \\ & - \mathbf{d}_2^T \mathbf{C}_2^{-1} \mathbf{A}_2 \boldsymbol{\lambda} + \mathbf{d}_2^T \mathbf{C}_2^{-1} \mathbf{d}_2) . \end{aligned} \quad (5)$$

If we let $\mathbf{Q} \equiv \mathbf{Q}_1 + \mathbf{Q}_2$, $\mathbf{Q}_i \equiv \mathbf{A}_i^T \mathbf{C}_i^{-1} \mathbf{A}_i$, $\mathbf{T} \equiv \mathbf{T}_1 + \mathbf{T}_2$, $\mathbf{T}_i \equiv \mathbf{A}_i^T \mathbf{C}_i^{-1} \mathbf{d}_i$ and group terms in powers of $\boldsymbol{\lambda}$, we can rewrite Eq. 5 as

$$E = -\frac{1}{2} (\boldsymbol{\lambda}^T \mathbf{Q} \boldsymbol{\lambda} - \boldsymbol{\lambda}^T \mathbf{T} - \mathbf{T}^T \boldsymbol{\lambda}) . \quad (6)$$

Here we ignore the two terms $\mathbf{d}_1^T \mathbf{C}_1^{-1} \mathbf{d}_1$ and $\mathbf{d}_2^T \mathbf{C}_2^{-1} \mathbf{d}_2$. These do not depend on $\boldsymbol{\lambda}$ and therefore do not affect the shape of $P(R)$. Since $\mathbf{C}_i^T = \mathbf{C}$, $\mathbf{Q}_i^T = \mathbf{Q}_i$ and $\mathbf{Q}^T = \mathbf{Q}$. This means that \mathbf{Q} is a Hermitian matrix, with real eigenvalues. So we make the assumption that it is invertible and change the form of E as

$$E = -\frac{1}{2} [(\boldsymbol{\lambda} - \mathbf{Q}^{-1} \mathbf{T})^T \mathbf{Q} (\boldsymbol{\lambda} - \mathbf{Q}^{-1} \mathbf{T}) - \mathbf{T}^T \mathbf{Q}^{-1} \mathbf{T}] . \quad (7)$$

Plugging it into Eq. 4 and integrating away $\boldsymbol{\lambda}$, we obtain the first major result of this paper,

$$P(R | \mathbf{d}_1, \mathbf{d}_2) \propto (\det \mathbf{Q})^{-1/2} \exp \left[\frac{1}{2} \mathbf{T}^T \mathbf{Q}^{-1} \mathbf{T} \right] P_{\text{prior}}(R) . \quad (8)$$

Here we have used the relation

$$G(\mathbf{Q}) \equiv \int \exp \left[-\frac{1}{2} \mathbf{z}^T \mathbf{Q} \mathbf{z} \right] \prod_{i=0}^N dz_i = (2\pi)^{N/2} (\det \mathbf{Q})^{-1/2} . \quad (9)$$

Notice that in Eq. 8, both \mathbf{Q} and \mathbf{T} depend on R , through $\mathbf{A}_2(R)$. There is no analytical expression for

the best-fit R , so we have to numerically evaluate $P(R)$. For the numerical evaluation, we should instead evaluate

$$\begin{aligned} \ln P(R | \mathbf{d}_1, \mathbf{d}_2) = & -\frac{1}{2} \ln (\det \mathbf{Q}(R)) + \ln P_{\text{prior}}(R) \\ & + \frac{1}{2} \mathbf{T}^T(R) \mathbf{Q}^{-1}(R) \mathbf{T}(R) + \text{const.} . \end{aligned} \quad (10)$$

To avoid numerical errors associated with too large/small exponential terms, a safer way is to evaluate the r.h.s. as a function of R , find the maximum, and then subtract this maximum before evaluating $P(R | \mathbf{d}_1, \mathbf{d}_2)$.

2.2. Correlated $\mathbf{d}_{1,2}$

The above result can be extended straightforwardly to the case of correlated $\mathbf{d}_{1,2}$. Now we define the data vector $\mathbf{d}^T = (\mathbf{d}_1, \mathbf{d}_2)$. The probability distribution of \mathbf{d} is

$$P(\mathbf{d} | R, \boldsymbol{\lambda}) = \frac{1}{\sqrt{(2\pi)^N \det \mathbf{C}}} \exp \left[-\frac{1}{2} \boldsymbol{\Delta}^T \mathbf{C}^{-1} \boldsymbol{\Delta} \right] . \quad (11)$$

Here $\boldsymbol{\Delta} \equiv \mathbf{d} - (\mathbf{A}_1 \boldsymbol{\lambda}, \mathbf{A}_2 \boldsymbol{\lambda})$. Because the errors in $\mathbf{d}_{1,2}$ are not independent, the covariance matrix \mathbf{C} includes the off-diagonal blocks. We denote

$$\mathbf{C} = \begin{pmatrix} \mathbf{C}_{11} & \mathbf{C}_{12} \\ \mathbf{C}_{21} & \mathbf{C}_{22} \end{pmatrix}, \mathbf{C}^{-1} = \begin{pmatrix} \mathbf{B}_{11} & \mathbf{B}_{12} \\ \mathbf{B}_{21} & \mathbf{B}_{22} \end{pmatrix}, \quad (12)$$

where $\mathbf{C}_{ij} = \langle \mathbf{n}_i \mathbf{n}_j^T \rangle$, and $\mathbf{C}_{12} = \mathbf{C}_{21}$. The blocks of inverse \mathbf{C} are

$$\begin{aligned} \mathbf{B}_{11} &= (\mathbf{C}_{11} - \mathbf{C}_{12} \mathbf{C}_{22}^{-1} \mathbf{C}_{21})^{-1}, \\ \mathbf{B}_{12} &= -(\mathbf{C}_{11} - \mathbf{C}_{12} \mathbf{C}_{22}^{-1} \mathbf{C}_{21})^{-1} \mathbf{C}_{12} \mathbf{C}_{22}^{-1}, \\ \mathbf{B}_{21} &= -\mathbf{C}_{22}^{-1} \mathbf{C}_{21} (\mathbf{C}_{11} - \mathbf{C}_{12} \mathbf{C}_{22}^{-1} \mathbf{C}_{21})^{-1}, \\ \mathbf{B}_{22} &= \mathbf{C}_{22}^{-1} + \mathbf{C}_{22}^{-1} \mathbf{C}_{21} (\mathbf{C}_{11} - \mathbf{C}_{12} \mathbf{C}_{22}^{-1} \mathbf{C}_{21})^{-1} \mathbf{C}_{12} \mathbf{C}_{22}^{-1}. \end{aligned} \quad (13)$$

The expansion of exponential part has 16 terms, which is twice as in Eq. 5. We define

$$\mathbf{Q}' \equiv \mathbf{A}_1^T \mathbf{B}_{11} \mathbf{A}_1 + \mathbf{A}_1^T \mathbf{B}_{12} \mathbf{A}_2 + \mathbf{A}_2^T \mathbf{B}_{21} \mathbf{A}_1 + \mathbf{A}_2^T \mathbf{B}_{22} \mathbf{A}_2, \quad (14)$$

$$\mathbf{T}' \equiv \mathbf{A}_1^T \mathbf{B}_{11} \mathbf{d}_1 + \mathbf{A}_1^T \mathbf{B}_{12} \mathbf{d}_2 + \mathbf{A}_2^T \mathbf{B}_{21} \mathbf{d}_1 + \mathbf{A}_2^T \mathbf{B}_{22} \mathbf{d}_2 . \quad (15)$$

We find that E in Eq. 4 is now

$$E = -\frac{1}{2} (\boldsymbol{\lambda}^T \mathbf{Q}' \boldsymbol{\lambda} - \boldsymbol{\lambda}^T \mathbf{T}' - \mathbf{T}'^T \boldsymbol{\lambda}) . \quad (16)$$

Therefore the final expression of $P(R | \mathbf{d}_1, \mathbf{d}_2)$ is identical to Eq. 8, but replacing \mathbf{Q} and \mathbf{T} with \mathbf{Q}' and \mathbf{T}' .

$$P(R | \mathbf{d}) \propto [\det \mathbf{Q}']^{-1/2} \exp \left[\frac{1}{2} \mathbf{T}'^T \mathbf{Q}'^{-1} \mathbf{T}' \right] P_{\text{prior}}(R) . \quad (17)$$

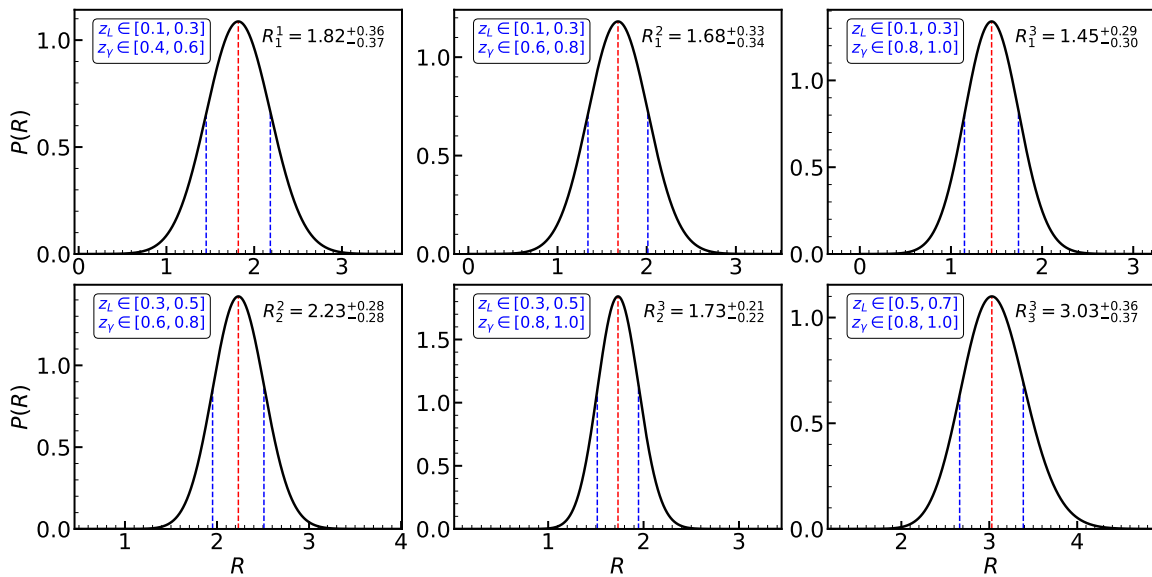


Figure 1. Measured posterior PDF $P(R)$ on the lensing ratios, using our ratio measurement method. $P(R)$ is nearly Gaussian. We also show the best-fit value and the associated 1σ errors. We take lenses as DESI galaxies at three redshift bins denoted by z_L . One of the sources is DECaLS cosmic shear at three redshift bins denoted by z_γ and the other is *Planck* CMB lensing.

Eq. 8 for uncorrelated $\mathbf{d}_{1,2}$ and Eq. 17 for correlated $\mathbf{d}_{1,2}$ are the major results of this paper. They provide the analytical expressions of $P(R)$. In order to put the two data sets on an equal footing, one should treat R and $1/R$ equally, which motivates a Jeffreys $1/R$ prior instead of flat prior¹.

3. APPLICATION: MEASURING THE LENSING RATIO

We have applied our method to measure the ratio between cross-correlations of galaxy-ISW and galaxy-CMB lensing (Dong et al. 2022), which is a measure of the gravitational potential decay rate and therefore a measure of dark energy. Here we take the lensing ratio measurement as another example to demonstrate the applicability of our method.

The two data sets that we adopt are $w^{g\gamma t}(\theta, z_L, z_\gamma)$ and $w^{g\kappa\text{CMB}}(\theta, z_L)$. $w^{g\gamma t}(\theta, z_L, z_\gamma)$ is the galaxy-tangential shear cross-correlation function between galaxies at lens redshift bin denoted by the mean redshift z_L and shear at source redshift bin denoted by the mean redshift z_γ . The corresponding galaxy-convergence cross-correlation function is denoted as $w^{g\kappa\gamma}(\theta, z_L, z_\gamma)$. $w^{g\kappa\text{CMB}}(\theta, z_L)$ is the galaxy-CMB lensing convergence cross-correlation function. It is expected that for narrow lens redshift bins (Jain & Taylor 2003; Bernstein & Jain 2004; Zhang et al. 2005),

$$w^{g\kappa\text{CMB}}(\theta, z_L) = R(z_L, z_\gamma)w^{g\kappa\gamma}(\theta, z_L, z_\gamma). \quad (18)$$

Notice that the lensing ratio $R(z_L, z_\gamma)$ depends on z_L and z_γ only through the geometry of the universe, but not structure growth. Measurement errors in $w^{g\gamma t}(\theta, z_L, z_\gamma)$ and $w^{g\kappa\text{CMB}}(\theta, z_L)$ are dominated by shear measurement errors and lensing map noises. So we will treat the two data sets as independent and apply Eq. 8 to measure the ratio R . Notice that we restrict the measurement to the CMB lensing/cosmic shear ratio and will not measure the shear ratio between shear at different source redshifts. In order not to divert readers into weak lensing details, we present the measurement of $w^{g\gamma t}(\theta, z_L, z_\gamma)$ and $w^{g\kappa\text{CMB}}(\theta, z_L)$ with DESI imaging surveys DR8, DECaLS shear catalog and *Planck* CMB lensing maps in Appendix A.

Since $w^{g\gamma t}$ and $w^{g\kappa\text{CMB}}$ involve different Bessel functions in the power spectrum-correlation function conversion ($J_2(\ell\theta)$ versus $J_0(\ell\theta)$), they are not proportional to each other. One way to deal with it in our method is to choose the theory λ as the power spectrum, and the mapping matrix $\mathbf{A}_{1,2}$ in Eq. 8 will then involve the oscillating functions of $J_{0,2}$. This is numerically challenging, even with the help of FFTlog (Hamilton 2000). For the purpose of demonstrating the usage of our method, we adopt a more convenient choice, that is to rescale the correlation functions $w \rightarrow \tilde{w} \equiv w/w_{\text{tem}}$. w_{tem} is the corresponding template correlation function based on the theoretical prediction of a fiducial cosmology (Eq. B10 & Eq. B11), which absorbs the $J_{0,2}$ dependences. Therefore, the rescaled correlation functions directly follow the proportionality relation ($\tilde{w}^{g\kappa\text{CMB}} = R\tilde{w}^{g\gamma t}$). There-

¹ Thanks the anonymous referee for this helpful suggestion.

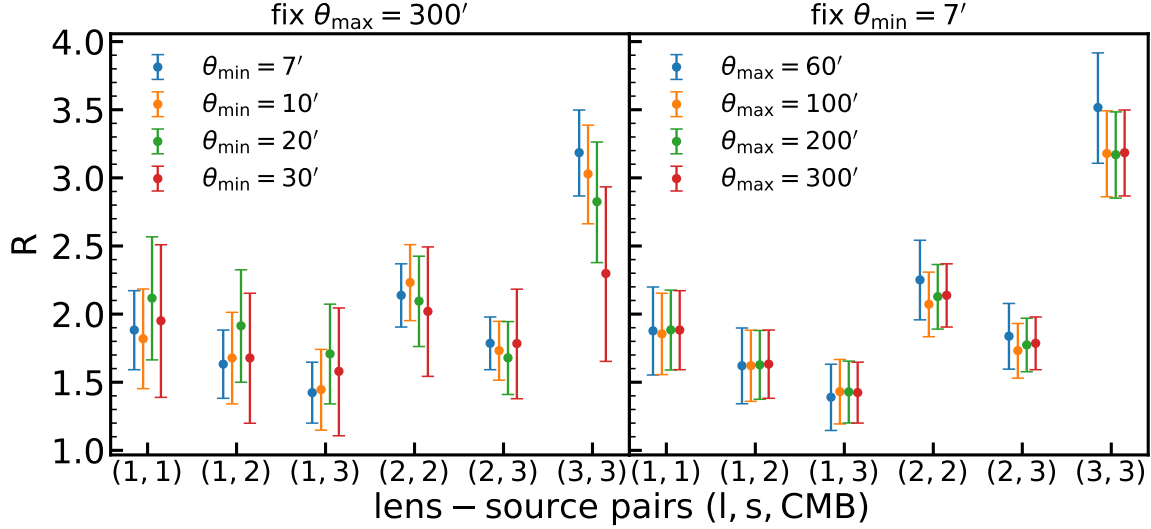


Figure 2. Consistency test 1. We find no statistically significant dependence of R on the chosen scale cut θ_{\min} (θ_{\max}).

fore we will use $\tilde{w}^{g\kappa_{\text{CMB}}}$ and $\tilde{w}^{g\gamma_t}$ as the data sets to demonstrate our ratio measurement method.

3.1. Measurements of lensing ratios

Following §2, we choose the data sets $\mathbf{d}_{1,2}$, the theory vector $\boldsymbol{\lambda}$, and the mapping matrixes $\mathbf{A}_{1,2}$ as

$$\begin{aligned} \mathbf{d}_1 &= \tilde{w}^{g\gamma_t}, \quad \mathbf{d}_2 = \tilde{w}^{g\kappa_{\text{CMB}}}, \\ \boldsymbol{\lambda} &= \langle \mathbf{d}_1 \rangle, \quad \mathbf{A}_1 = \mathbf{I}, \quad \mathbf{A}_2 = R\mathbf{I}. \end{aligned} \quad (19)$$

Since the theory vector $\boldsymbol{\lambda}$ is just the expectation value of \mathbf{d}_1 , the theory makes no assumptions on cosmology and the measured R will be model independent. We have three lens bins ($0.1 < z_L < 0.3$, $0.3 < z_L < 0.5$ and $0.5 < z_L < 0.7$) and three source shear bins ($0.4 < z_\gamma < 0.6$, $0.6 < z_\gamma < 0.8$ and $0.8 < z_\gamma < 1.0$). We denote the lens bins with Latin letter $i = 1, 2, 3$ and source bins with Greek letter $\alpha = 1, 2, 3$. Since we only measure the ratio between CMB lensing and cosmic shear, we have six ratios ($R_i^\alpha = R_1^1, R_1^2, R_1^3, R_2^2, R_2^3$ and R_3^3). We use the data in the range $10 < \theta < 300$ arcmin to measure the ratios.

Fig. 1 shows the posterior $P(R)$, which is normalized such that $\int P(R)dR = 1$. $P(R)$ is nearly Gaussian, resulting in $R_1^1 = 1.82^{+0.36}_{-0.37}$, $R_1^2 = 1.68^{+0.33}_{-0.34}$, $R_1^3 = 1.45^{+0.29}_{-0.30}$, $R_2^2 = 2.23^{+0.28}_{-0.28}$, $R_2^3 = 1.73^{+0.21}_{-0.22}$, $R_3^3 = 3.03^{+0.36}_{-0.37}$. The S/N of each ratio is between 4.9 and 8.4. The error budget is dominated by errors in the galaxy-CMB lensing correlation measurement. Therefore errors in R_1^1 , R_1^2 and R_1^3 are tightly correlated, since they share the same galaxy-CMB lensing measurement. So are errors in R_2^2 and R_2^3 . Meanwhile, we test our method for multiple correlated $\mathbf{R}_1^\alpha = \text{diag}(R_1^1, \dots, R_1^2, \dots, R_1^3, \dots)$ and $\mathbf{R}_2^\alpha = \text{diag}(R_2^2, \dots, R_2^3, \dots)$. We take the vector of $\tilde{w}^{g\gamma_t}$ in the identical lens bin as \mathbf{d}_1 , and the vector of $\tilde{w}^{g\kappa_{\text{CMB}}}$

in the identical lens bin as \mathbf{d}_2 . For example, $\mathbf{d}_1 = (\tilde{w}_1^{g\gamma_t,1}, \tilde{w}_1^{g\gamma_t,2}, \tilde{w}_1^{g\gamma_t,3})$, $\mathbf{d}_2 = (\tilde{w}_1^{g\kappa_{\text{CMB}}}, \tilde{w}_1^{g\kappa_{\text{CMB}}}, \tilde{w}_1^{g\kappa_{\text{CMB}}})$. The theory vector $\boldsymbol{\lambda} = \langle \mathbf{d}_1 \rangle$, and the mapping matrixes $\mathbf{A}_1 = \mathbf{I}$, $\mathbf{A}_2 = R_1^\alpha \mathbf{I}$. The measured ratios are identical with those shown in Fig. 1.

3.2. Consistency checks

To demonstrate the validity of our method and measurement, we perform several consistency checks.

We first check whether the constrained R depends on the chosen θ range ($\theta_{\min} < \theta < \theta_{\max}$). By theoretical design, the ratio R is scale-independent. Therefore the measured R should be independent of scale cuts. Nonetheless, the correlation function measurements themselves may suffer from potential systematics in the galaxy clustering, shear, and CMB lensing. The left panel of Fig. 2 shows the consistency tests by varying $\theta_{\min} = 7', 10', 20', 30'$ while fixing $\theta_{\max} = 300'$. The right panel shows the tests by varying $\theta_{\max} = 60', 100', 200', 300'$ while fixing $\theta_{\min} = 7'$. The constrained R are fully consistent with each other. The left panels show a larger scatter in R , since a small scale cut affects the overall S/N more significantly.

The second check is to compare against the direct model fitting result introduced in §A.4. This method adopts the *Planck* cosmology predicted w up to a scale-independent amplitude b and fit b for both $w^{g\gamma_t}$ and $w^{g\kappa_{\text{CMB}}}$. The ratio is then $R^{\text{fit}} = b_{\text{fit}}^{g\kappa_{\text{CMB}}} / b_{\text{fit}}^{g\gamma_t}$. The error of R^{fit} is

$$\Delta R^{\text{fit}} = \frac{b_{\text{fit}}^{g\kappa_{\text{CMB}}}}{b_{\text{fit}}^{g\gamma_t}} \sqrt{\left(\frac{\sigma_b^{g\kappa_{\text{CMB}}}}{b_{\text{fit}}^{g\kappa_{\text{CMB}}}}\right)^2 + \left(\frac{\sigma_b^{g\gamma_t}}{b_{\text{fit}}^{g\gamma_t}}\right)^2}. \quad (20)$$

The values of R^{fit} are $R_1^{1,\text{fit}} = 1.87 \pm 0.36$, $R_1^{2,\text{fit}} = 1.68 \pm 0.32$, $R_1^{3,\text{fit}} = 1.46 \pm 0.28$, $R_2^{2,\text{fit}} = 2.32 \pm 0.28$, $R_2^{3,\text{fit}} =$

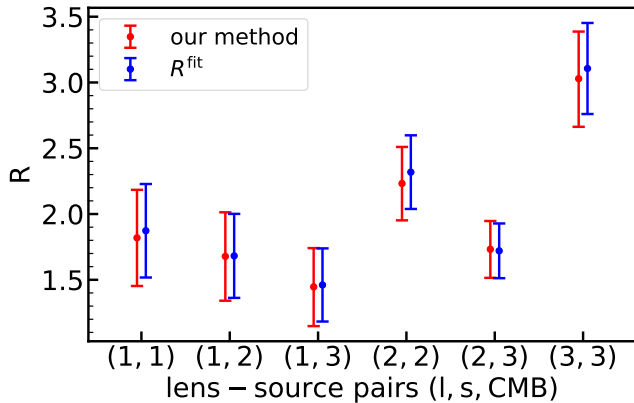


Figure 3. Consistency test 2. We compare the measured R by our method with R^{fit} from model fitting.

1.72 ± 0.21 , $R_3^{3,\text{fit}} = 3.11 \pm 0.35$. As shown in Appendix A.4, this one-parameter bias model describes the measured correlation functions well, and confirms the robustness of the cross-correlation measurement. Therefore the ratio obtained in this way provides a robust check of R measured by our method. Fig. 3 shows the two results (best-fit values and the associated errors) are fully consistent with each other. Our method, without the assumption of scale-independent bias, can be directly applied to smaller angular scales, where scale dependence of bias may be non-negligible.

The third test is on the potential cosmological dependence that we introduce by the scaling $w \rightarrow w/w_{\text{tem}}$, which is a convenient but not exact implementation of our method. We measure the lensing ratio adopting different cosmologies (the first year (Spergel et al. 2003), five-year (Komatsu et al. 2009), nine-year WMAP cosmology (Hinshaw et al. 2013) and Planck 2018 cosmology (Planck Collaboration et al. 2020a) in Table. 1) and corresponding template of scaling. Fig. 4 shows that, despite various differences in cosmological parameters, the differences in the measured R are all smaller than 0.5σ and therefore are totally negligible.

Parameter	Ω_c	Ω_b	n_s	H_0	σ_8
WMAP1	0.224	0.0463	0.99	72	0.9
WMAP5	0.206	0.0432	0.961	72.4	0.787
WMAP9	0.235	0.0464	0.9710	69.7	0.820
Planck18	0.265	0.04887	0.9649	67.36	0.8111

Table 1. The first year (Spergel et al. 2003), five-year (Komatsu et al. 2009), nine-year WMAP cosmology (Hinshaw et al. 2013), and Planck 2018 cosmology (Planck Collaboration et al. 2020a).

4. CONCLUSIONS

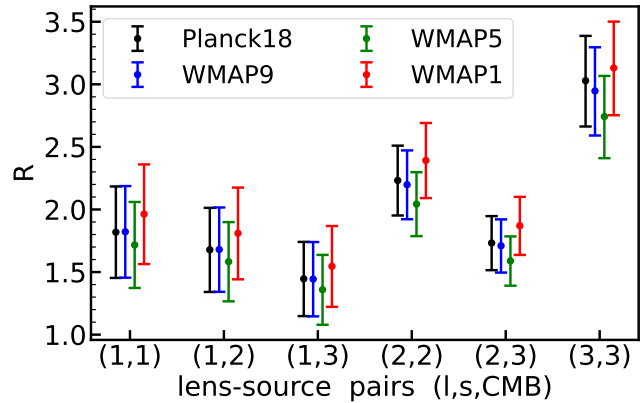


Figure 4. Consistency test 3. The measured R has negligible dependence on the adopted theoretical template, which depends on cosmology.

We develop an unbiased method to solve the problem of measuring the ratio of two data sets. This solution is developed based on Bayesian analysis, including all the data points and their uncertainties. The posterior distribution of the ratio $P(R)$ has an analytical expression. This method enables fast and unbiased R measurement, with minimal statistical errors. Furthermore, it relies on the usual assumption of Gaussian error in data, but no underlying model other than the proportionality relation between the two data sets.

We measure the lensing ratio as an application. We take the lenses as DESI imaging survey galaxies, and sources as DECaLS cosmic shear and Planck CMB lensing. We measure the ratio between CMB lensing and cosmic shear at multiple lens-source redshift pairs, with S/N ranging from 5 to 8. We verify that the measured R is insensitive to the scale cuts and the adopted cosmology. Together with another example of measuring the decay rate of cosmological gravitational potential (Dong et al. 2022), we demonstrate the applicability of our method to measure the ratios.

ACKNOWLEDGEMENTS

This work is supported by the National Science Foundation of China (11621303), the National Key R&D Program of China (2020YFC2201602, 2018YFA0404504, 2018YFA0404601, 2020YFC2201600) and CMS-CSST-2021-A02. J.Y. acknowledges the support from China Postdoctoral Science Foundation (2021T140451). H.Y.S. acknowledges the support from CMS-CSST-2021-A01, NSFC of China under grant 11973070, and Key Research Program of Frontier Sciences, CAS, grant No. ZDBS-LY-7013. This work made use of the Gravity Supercomputer at the Department of Astronomy, Shanghai Jiao Tong University. The results in this paper have been derived using the following packages: Numpy

(van der Walt et al. 2011), HEALPix (Górski et al. 2005), IPython (Perez & Granger 2007), CCL (Chisari et al. 2019), and TreeCorr (Jarvis et al. 2004).

DATA AVAILABILITY

APPENDIX

A. DATA PRE-PROCESSING

We introduce the data that we use to measure the cross-correlation functions of galaxy-tangential shear, and galaxy-CMB lensing. These cross-correlations will then be used by our ratio estimator as the input.

A.1. *The lens galaxy catalog*

For the lens galaxies, we choose DESI imaging survey DR8 (Dark Energy Camera Legacy Survey; Dey et al. 2019). We also use the photometric redshift measurement provided by Zou et al. (2019). This catalog also applies to other cosmological analyses (e.g. Yao et al. (2020); Zhang et al. (2021b); Dong et al. (2021); Zou et al. (2021)). The imaging footprints cover an area of over 14,000 deg² in both northern and southern Galactic caps. The catalog contains about 0.17 billion morphologically classified galaxies with $r < 23$ mag and covers the redshift range of $z^P < 1$.

We select the lens galaxies in three redshift bins of $0.1 < z_L < 0.3$, $0.3 < z_L < 0.5$ and $0.5 < z_L < 0.7$, with r -band apparent magnitude cut of 18.5, 19.5, 20.5 at each bin respectively. The final catalog contains $\sim 3.64, 2.59, 2.20$ million galaxies in each bin and ~ 8.43 million in total. To select the random galaxies² with considering the survey geometry, we first generate a mask of lens galaxies, with $n_{\text{side}} = 512$ in HEALPix (Górski et al. 2005). The binary tracer mask is 1 when there are tracer galaxies located at the pixel; otherwise it is 0. The random galaxies have an identical mask to the tracer galaxies.

A.2. *The weak lensing catalogs*

For weak lensing, we use two data sets. One is the shear catalog derived from the DECaLS images of DR8. The shear catalog models potential biases with a multiplicative and an additive bias (Heymans et al. 2012; Miller et al. 2013). The shear measurement and imperfect modeling of point-spread function (PSF) size result in the multiplicative bias. To calibrate our shear catalog, we cross-matched the DECaLS DR8 objects with the external shear measurements, including Canada-

The Python code, Jupyter notebooks, and the data files for reproducing the results and figures of this work can be found on Github at https://github.com/Ze-yangSUN/Ratio_method.

France-Hawaii Telescope (CFHT) Stripe 82, Dark Energy Survey (DES; Dark Energy Survey Collaboration et al. 2016) and Kilo-Degree Survey (KiDS; Hildebrandt et al. 2017). The additive bias comes from residuals in the anisotropic PSF correction which depends on galaxy sizes. The additive bias is subtracted from each galaxy in the catalog. The DECaLS DR8 shear catalog was used in the cluster weak lensing measurement by Zu et al. (2021), and the same shear catalog and photo- z measurements (but from DECaLS DR3) were used in the weak lensing analysis of intrinsic alignment studies of Yao et al. (2020), and CODEX clusters by Phriksee et al. (2020), and we refer readers to these two papers for technical details of the DECaLS shear catalog and photo- z errors. The shear catalog contains ~ 43.9 million galaxies covering $\sim 15,000$ deg². We split it into three redshift bins of $0.4 < z_\gamma < 0.6$, $0.6 < z_\gamma < 0.8$, $0.8 < z_\gamma < 1.0$. These bins have 26.9, 11.8, 5.18 million source galaxies respectively.

Another lensing data is the latest *Planck* CMB lensing convergence maps with corresponding mask (Planck Collaboration et al. 2020b,a). As we have found in our previous work of DESI galaxy group-Planck CMB lensing cross-correlation (Sun et al. 2022), the residual thermal Sunyaev-Zel'dovich (SZ) effect contaminates the lensing map and biases the cross-correlation measurement. So in the current analysis we adopt the CMB lensing map reconstructed from the tSZ-deprojected temperature-only SMICA map³ (Planck Collaboration et al. 2020b). The spherical harmonic coefficients of lensing convergence are provided in HEALPix with $\ell_{\text{max}} = 4096$, and the associated mask is provided with the resolution $n_{\text{side}} = 2048$. Due to the overwhelming reconstruction noise at small scales, the κ map was filtered to remove modes with $\ell > 1536$. Since we focus on large-scale clustering, we downgraded the κ map to $n_{\text{side}} = 512$ with $\ell_{\text{max}} = 1536$.

A.3. *Measurements of the correlation functions*

We measure the angular two-point correlation function between the pixelized CMB lensing convergence

² <https://www.legacysurvey.org/dr8/files/#random-catalogs>

³ <http://pla.esac.esa.int/pla/#cosmology>

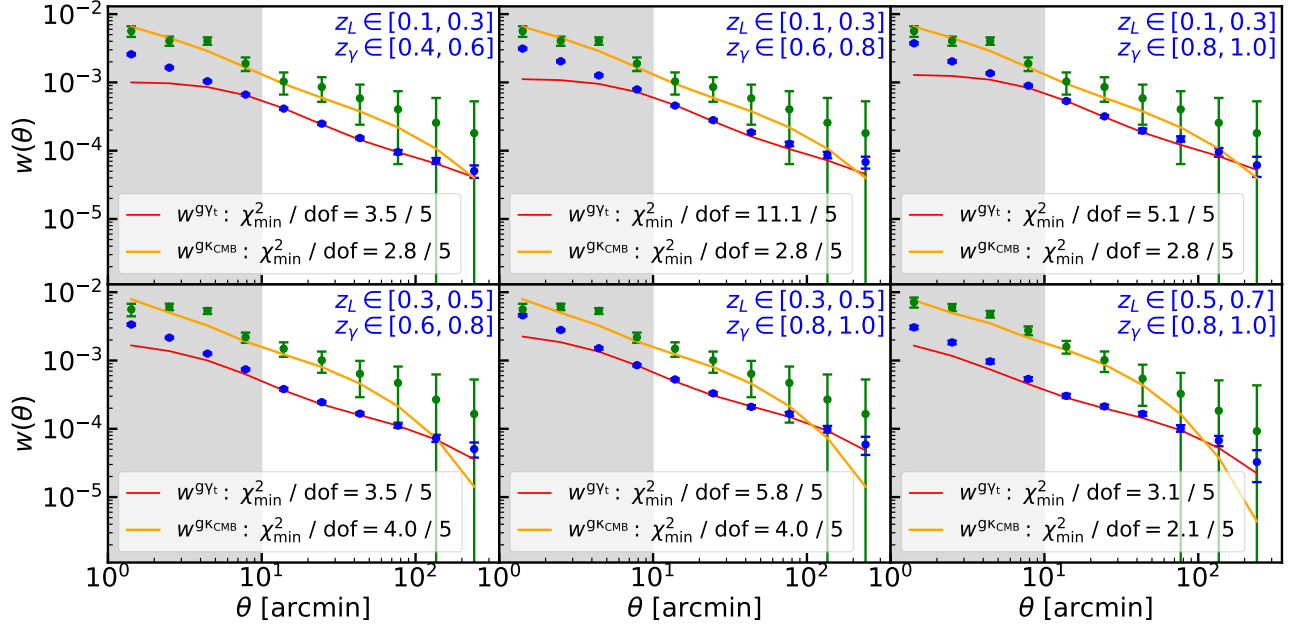


Figure 5. Measurements of galaxy-shear cross-correlation ($w^{g\gamma_t}$) and galaxy-CMB lensing cross-correlation ($w^{g\kappa_{CMB}}$) for various lens-source pairs, together with the best-fitting theory curves. The gray areas ($\theta < 10'$) correspond to the scales that are not used in the lensing ratio measurement.

map κ_{CMB} and the galaxy overdensity δ_g by summing over tracer-convergence pixel pairs g , separated by angle θ . We subtract the corresponding correlation with a sample of random points in place of the tracer galaxies, where the sum is over random-convergence pairs r separated by θ . The final estimator is

$$w^{g\kappa_{CMB}}(\theta) = \frac{\sum_g \omega_g \kappa_g(\theta)}{\sum_g \omega_g} - \frac{\sum_r \omega_r \kappa_r(\theta)}{\sum_r \omega_r}, \quad (\text{A1})$$

where ω_g and ω_r are the weights associated respectively with each tracer galaxy and random point. For the random points we set $\omega_r = 1$, and for the galaxies we set $\omega_g = 1$ without considering the observational systematics. This estimator is analogous to that used in tangential shear measurements in galaxy-galaxy lensing, which is

$$w^{g\gamma_t} = \frac{\sum_{ED} w_j \gamma_j^+}{\sum_{ER} (1 + m_j) w_j}, \quad (\text{A2})$$

where \sum_{ED} means summing over all the tangential ellipticity (E)-galaxy count in the data (D) pairs, \sum_{ER} means summing over all the tangential ellipticity (E)-galaxy count in the random catalog (R) pairs. The random catalog aims to subtract the selection bias in the correlation function from the shape of the footprint of the survey. Besides, w_j denotes the *lensfit* (Miller et al. 2013) weight for the galaxy shape measurement; γ_j^+ is the tangential ellipticity for the j th galaxy; m_j is the estimation of multiplicative bias provided by the same catalog.

For the fiducial measurements in this work, we group the tracer-convergence / tracer-shear pairs in 10 log-spaced angular separation bins between $1'$ and $300'$. We use *treecorr* (Jarvis et al. 2004) to measure all two-point correlation functions and covariance matrices. We estimate the covariance matrix between the measurements using the jackknife method. In this approach, the survey area is divided into 100 regions ('jackknife patches'), and the correlation function measurements are repeated once with each jackknife patch removed for the tracer as well as the lensing sample. The measured correlation functions between galaxy-galaxy lensing or galaxy-CMB lensing are shown as a function of angular scale in Fig. 5.

A.4. Evaluating the S/N of correlation measurements

We first quantify the detection significance of a non-zero signal, $(S/N)^2 \equiv \chi_{\text{null}}^2$. Here

$$\chi_{\text{null}}^2 = \sum_{\theta\theta'} w_{\text{obs}}(\theta) \mathbf{Cov}_{\theta\theta'}^{-1} w_{\text{obs}}(\theta'). \quad (\text{A3})$$

$w_{\text{obs}}(\theta)$ is for observation data, and $\mathbf{Cov}_{\theta\theta'}$ is the covariance matrix via the jackknife method. The detections are significant at all six lens-source pairs, $S/N = 30.7, 30.5, 28.2, 31.5, 31.0, 19.3$ for 11, 12, 13, 22, 23, 33 galaxy-shear pairs, their total S/N is 70.7. $S/N = 5.6, 8.8, 10.2$ for galaxy- κ_{CMB} from low to high redshift, respectively, their total S/N is 14.6. To evaluate the above S/N , we use the data in the range $10' < \theta < 300'$. Therefore the error budget of lensing ratio measurement

is dominated by that in galaxy-CMB lensing, which is in turn dominated by noises in the CMB lensing map.

We further check whether the measurements agree with our theoretical expectation, by the goodness of fitting. We approximate the galaxy bias defined through $b_g(k) \equiv P_{gm}(k)/P_m(k)$ as scale-independent. Here P_m is the nonlinear matter power spectrum. Under this approximation, $C^{g\kappa} = bC^{m\kappa}$. We fix the cosmology as *Planck* 2018 cosmology (Planck Collaboration et al. 2020a): $\Omega_m = 0.315, \Omega_\Lambda = 0.685, n_s = 0.965, h = H_0/(100 \text{ km s}^{-1} \text{ Mpc}^{-1}) = 0.674$ and $\sigma_8 = 0.811$. We then compute $C^{m\kappa}$ using the Core Cosmology Library (CCL; Chisari et al. (2019)). We then convert $C^{g\kappa}$ into $w^{g\gamma_t}$ and $w^{g\kappa_{\text{CMB}}}$ with FFTLog in `pyccl` (Chisari et al. 2019). Since in the CMB lensing correlation measurement we have filtered away modes $\ell \gtrsim 1536$ to suppress measurement noise, we adopt the same maximum $\ell_{\text{max}} = 1536$ cut in the integral of Eq. B9. We then have the theoretical template for the one-parameter fitting, $w = bw_{\text{tem}}$ (Eq. B10 & Eq. B11). We adopt the same power spectrum for generating $w_{\text{tem}}^{g\gamma_t}$ and $w_{\text{tem}}^{g\kappa}$. So Fig. 5 also shows the best-fit theoretical curves. Since the constant bias approximation only holds at relatively large scale, we take a scale cut $10' < \theta < 300'$, resulting in satisfying $\chi_{\text{min}}^2/\text{d.o.f.} \lesssim 1$ (Fig. 5). We are then confident that at least within this scale range, the measurements have insignificant contamination.

B. THE LENSING RATIO STATISTICS

The lensing convergence κ , in the direction $\boldsymbol{\theta}$ is given by

$$\kappa(\boldsymbol{\theta}) = \int_0^\infty d\chi W(\chi) \delta(\boldsymbol{\theta}, \chi). \quad (\text{B4})$$

Here $\delta(\chi, \boldsymbol{\theta})$ is the density fluctuations at sky position $\boldsymbol{\theta}$. $W(\chi)$ is the κ kernel. The one corresponding to the galaxy shear catalog is

$$W^\gamma(\chi) = \frac{3}{2} \Omega_{m0} H_0^2 (1+z) \int_\chi^\infty d\chi' n_\gamma(\chi') \frac{d_A(\chi) d_A(\chi, \chi')}{d_A(\chi')}. \quad (\text{B5})$$

Here Ω_{m0} is the matter density today, H_0 is the Hubble constant today, χ is the comoving distance to redshift z , $d_A(\chi)$ is the angular diameter distance to χ , $d_A(\chi, \chi')$ is the angular diameter distance between comoving distance χ and χ' , and $n_\gamma(\chi)$ represents the normalized distribution of source shear galaxies.

For CMB lensing, the source distribution can be approximated as a Dirac δ_D function centered at the comoving distance to the surface of last scattering, $\chi^* = \chi(z^* \approx 1090)$. In this case, the lensing kernel W is given by

$$W^{\text{CMB}}(\chi) = \frac{3}{2} \Omega_{m0} H_0^2 (1+z) \frac{d_A(\chi) d_A(\chi, \chi^*)}{d_A(\chi^*)}. \quad (\text{B6})$$

Using the Limber approximation (Limber 1953) and the flat sky approximation, the galaxy overdensity-lensing cross power spectrum is

$$C^{g\kappa}(\ell) = \frac{2\pi^2}{\ell^3} \int d\chi n_L(z) W(\chi) d_A(\chi) \Delta_{\text{gm}}^2 \left(k = \frac{\ell + 1/2}{d_A(\chi)}, z \right). \quad (\text{B7})$$

Here $\Delta_{\text{gm}}^2(k) = k^3 P_{\text{gm}}(k)/(2\pi^2)$ and P_{gm} is the 3D galaxy-matter cross power spectrum. $n_L(z)$ is the redshift distribution for the lens galaxies. Notice that $W(\chi)$ can either be $W^\gamma(\chi)$ or W^{CMB} . The corresponding galaxy-tangential shear cross-correlation and galaxy-CMB lensing convergence cross-correlation functions are

$$w^{g\gamma_t}(\theta) = \int_0^\infty \frac{\ell d\ell}{2\pi} J_2(\ell\theta) C^{g\kappa_\gamma}(\ell), \quad (\text{B8})$$

$$w^{g\kappa_{\text{CMB}}}(\theta) = \int_0^\infty \frac{\ell d\ell}{2\pi} J_0(\ell\theta) C^{g\kappa_{\text{CMB}}}(\ell). \quad (\text{B9})$$

Here J_0 and J_2 are the zero- and second-order Bessel functions of the first kind, respectively. J_2 , instead of J_0 , shows up in Eq. B8, since shear is a spin-2 field and only the tangential shear is correlated with the galaxy distribution (scalar field).

The corresponding template correlation functions w_{tem} of above two cross-correlations are

$$w_{\text{tem}}^{g\gamma_t}(\theta) = \int_0^{\ell_{\text{max}}} \frac{\ell d\ell}{2\pi} J_2(\ell\theta) C_{\text{tem}}^{g\kappa_{\text{CMB}}}(\ell), \quad (\text{B10})$$

$$w_{\text{tem}}^{g\kappa_{\text{CMB}}}(\theta) = \int_0^{\ell_{\text{max}}} \frac{\ell d\ell}{2\pi} J_0(\ell\theta) C_{\text{tem}}^{g\kappa_{\text{CMB}}}(\ell). \quad (\text{B11})$$

It should be noted that $w_{\text{tem}}^{g\gamma_t}$ is not converted from its corresponding power spectrum $C_{\text{tem}}^{g\kappa_\gamma}$ in Eq. B10. Because we adopt the same power spectrum $C_{\text{tem}}^{g\kappa_{\text{CMB}}}$ for generating $w_{\text{tem}}^{g\gamma_t}$ and $w_{\text{tem}}^{g\kappa_{\text{CMB}}}$. This causes the rescaled correlation functions $\tilde{w}(\equiv w/w_{\text{tem}})$ to follow the proportionality relation $\tilde{w}^{g\kappa_{\text{CMB}}} = R\tilde{w}^{g\gamma_t}$.

B.1. Modeling the lensing ratio

For the same lens sample of sufficiently narrow redshift distribution, we expect

$$R = \frac{C^{g\kappa_{\text{CMB}}}}{C^{g\kappa_\gamma}} = \frac{W^{\text{CMB}}(\bar{\chi}_L)}{W^\gamma(\bar{\chi}_L)}. \quad (\text{B12})$$

Here $\bar{\chi}_L$ is the mean radial coordinate of lens galaxies. The ratio does not depend on the matter clustering and complexities associated with it, so it provides a clean measure of cosmic distances. The key here is the cancellation of the galaxy-matter power spectra in Eq. B7 & Eq. B12. This requires that the lens galaxies are narrowly distributed in redshift space. Under such a limit,

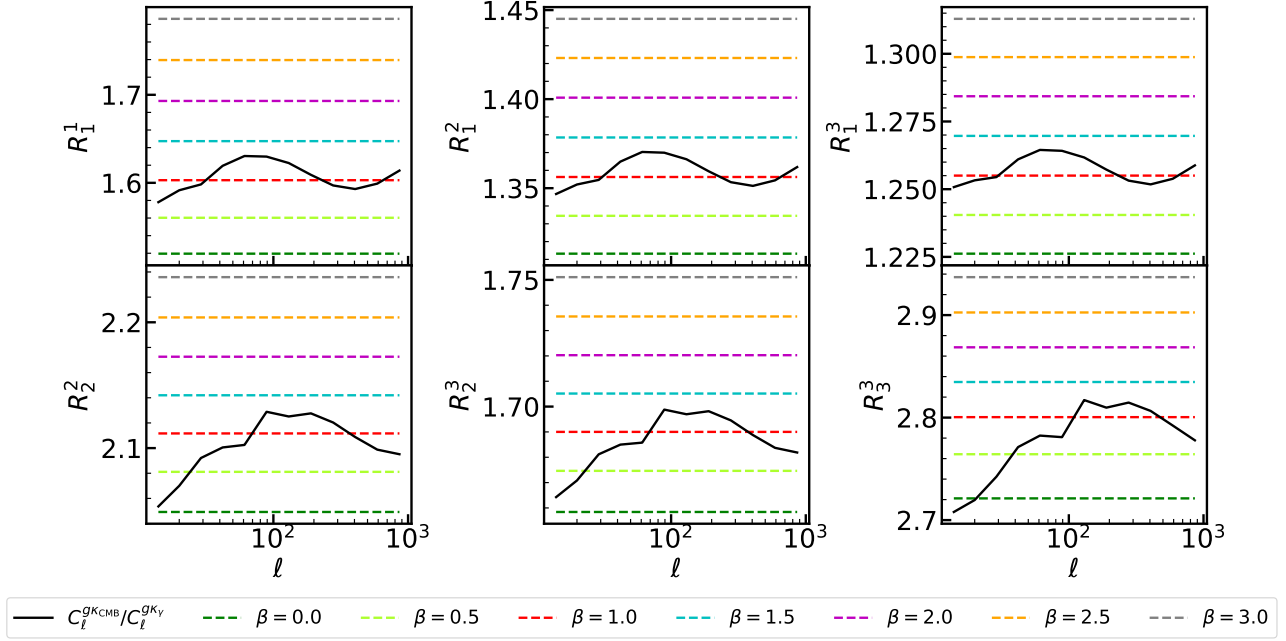


Figure 6. The exact lensing ratio ($C_{\ell}^{gK_{\text{CMB}}}/C_{\ell}^{gK_{\gamma}}$) and its modeling (Eq. B13 with different values of β). Eq. B13 with $\beta = 1.0$ provides an excellent approximation of the lensing ratio.

the power spectrum can be well approximated as a constant and can be moved outside of the integral. This approximation breaks to a certain extent in our analysis, since the photometric redshift width is $\Delta z_L^P = 0.2$ and the true redshift width is expected to be larger. Scrutinizing Eq. B7 & Eq. B12, we expect

$$R = \frac{\int_0^{\infty} (1+z) \frac{d_L d_{LCMB}}{d_{CMB}} n_L(z) \chi^{-2+\beta} dz}{\int_0^{\infty} (1+z) d_L n_L(z) \chi^{-2+\beta} dz \frac{\int_0^{\infty} \frac{d_L \gamma}{d_{\gamma}} n_{\gamma}(z_{\gamma}) dz_{\gamma}}{\int_0^{\infty} n_{\gamma}(z_{\gamma}) dz_{\gamma}}}. \quad (\text{B13})$$

Here the parameter β and the associated function $\chi^{-2+\beta}$ are to weigh the contribution from each redshift. $\beta = 0$ corresponds to approximate $P_{\text{gm}}(k = \ell/d_A(z), z)$ in the integrals of Eq. B7 & Eq. B12 as redshift independent, for fixed ℓ . $\beta = 3$ corresponds to approximate $\Delta_{\text{gm}}^2(k = \ell/d_A(z), z)$ as redshift independent. There is no guarantee on either choice of β . So we try various values of parameter $\beta \in [0, 3]$ and compare with R calculated as $C^{gK_{\text{CMB}}}/C^{gK_{\gamma}}$. Fig. 6 shows that the choice of $\beta = 1$ is nearly exact. This choice of $\beta = 1$ is insensitive to the redshift pairs, as shown in the same figure. Furthermore, we have tested that even if we enlarge the adopted photo- z error by a factor of 2, $\beta = 1$ remains the most accurate. Therefore, we adopt $\beta = 1.0$ throughout this work to calculate the theoretical expectation value of ratios.

B.2. Implications of the ratio measurement

We now proceed to the comparison between the measured R and the theoretical prediction of the fiducial

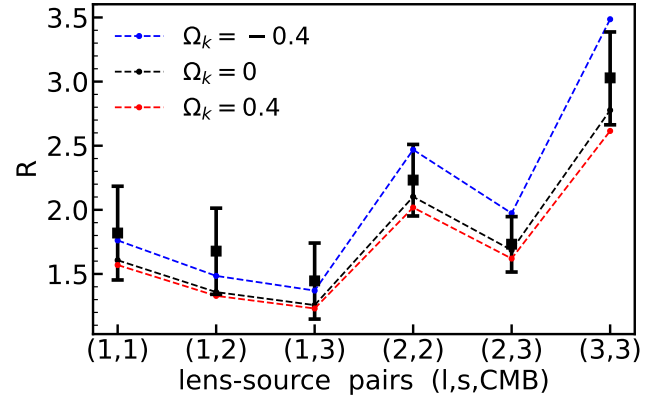


Figure 7. The impact of curvature Ω_k on the lensing ratios R . The negative value of Ω_k has a significantly greater impact on the lensing ratios than the positive value.

flat *Planck* 2018 cosmology. Fig. 7 shows that the two agree with each within the measurement statistical error bars. Nevertheless, the theory seems systematically lower than the data. The difference is 17% in R_1^1 , R_1^2 & R_1^3 , 4% in R_2^2 & R_2^3 , and 8% in R_3^3 . Although the significance of the overall discrepancy is only $\Delta\chi^2 = 1.04$.⁴ If we parameterize the differences into an overall amplitude A through $R = AR_{\text{Planck}}$, $A = 1.08 \pm 0.09$. [Prat et al. \(2019\)](#) measured the lensing ratios using galaxy

⁴ Notice that errors of the first three data points are tightly correlated. So are the next two data points. Therefore effectively we have only three independent data points.

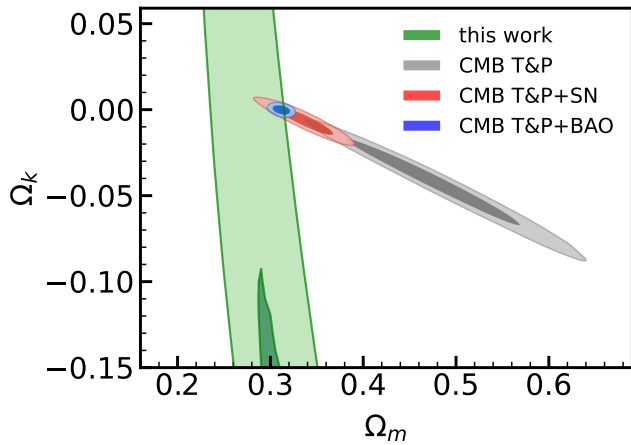


Figure 8. Cosmological constraint under the assumption of a model with a $w = -1$ cosmological constant with free curvature. The $\Omega_m - \Omega_k$ constraint uses the six measured lensing ratios (green), CMB (gray), CMB + SN (red), and CMB + BAO (blue).

position and lensing data from DES, and CMB lensing data from the SPT+*Planck*. They found a best-fitting lensing ratio amplitude of $A = 1.1 \pm 0.1$. Our result of amplitude fitting is consistent with the previous work.

It is beyond the scope of this paper to fully investigate the above issues. Instead, we briefly discuss two possibilities. One possibility is that the universe is non-flat. Fig. 7 explores this possibility by varying Ω_K , while fixing all other cosmological parameters to the *Planck* 2018 (Planck Collaboration et al. 2020a). R indeed varies with Ω_K . However, the required modification of Ω_K ($\Omega_K \rightarrow -0.4$) is likely too dramatic to explain the data. Fig. 8 shows our result of the $\Omega_m - \Omega_k$ constraint compared with eBOSS cosmology (Alam et al. 2021). Using six lensing ratios leads to a detection of $\Omega_m = 0.28^{+0.05}_{-0.07}$. The measured ratios do not provide a strong constraint on the cosmological curvature.

Another possibility is the redshift uncertainties in the lens redshift and/or shear source redshift, as noticed in previous works (e.g. Das & Spergel (2009); Kitching et al. (2015); Prat et al. (2019)). Because of this, shear ratios can cross-check the redshift distributions. This has been done in the Sloan Digital Sky Survey (SDSS, Mandelbaum et al. 2005), where both redshifts and multiplicative shear biases were tested for the first time. Afterwards, in the Kilo-Degree Survey (KiDS, Giblin et al.

2021; Heymans et al. 2012; Hildebrandt et al. 2017, 2020; Asgari et al. 2021) and in Dark Energy Survey (DES, Davis et al. 2017; Omori et al. 2019; Sánchez et al. 2021; Abbott et al. 2022) tested the redshift uncertainties are ~ 0.01 . But DECaLS shape catalog we used in this analysis has not done this yet.

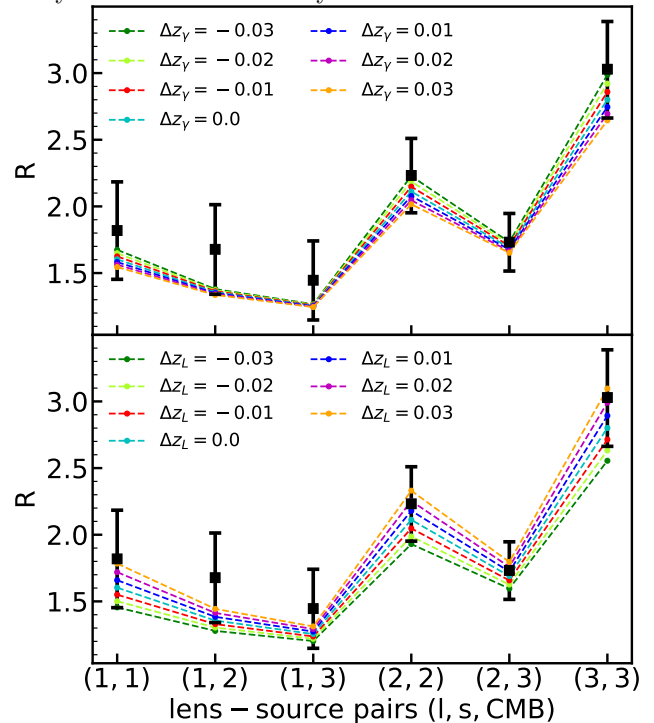


Figure 9. The impact of lens (shear source) redshift bias on the lensing ratios.

Redshift uncertainties can show as the r.m.s. σ_z of the estimated z^P or as a systematic bias Δz (Baxter et al. 2019; Prat et al. 2019). (1) The mean σ_z of tracer galaxies is $\sim 0.019, 0.034, 0.043$ at redshift bin 0.1-0.3, 0.3-0.5, 0.5-0.7, respectively. Doubling σ_z only affects R by less than 4%. Thus, σ_z is not the major reason for the $\sim 10\%$ overestimation of ratios. (2) Δz changes the redshift distribution from $n^i(z)$ to $n^i(z + \Delta z)$ (Eq. B13). Fig. 9 shows the theoretical prediction of its impact. Positive Δz_L for lens samples, or negative Δz_γ for shear samples, are more consistent with the measured lensing ratio. $\Delta z \sim 0.01 - 0.03$ is sufficient to explain the found overestimation of R . Therefore the possible bias in the mean redshift should be included to correctly interpret the lensing ratio measurement.

REFERENCES

Abbott, T. M. C., Aguena, M., Alarcon, A., et al. 2022, *PhRvD*, 105, 023520, doi: 10.1103/PhysRevD.105.023520

Addison, G. E., Bennett, C. L., Jeong, D., Komatsu, E., & Weiland, J. L. 2019, *ApJ*, 879, 15, doi: 10.3847/1538-4357/ab22a0

- Alam, S., Miyatake, H., More, S., Ho, S., & Mandelbaum, R. 2017, *MNRAS*, 465, 4853, doi: [10.1093/mnras/stw3056](https://doi.org/10.1093/mnras/stw3056)
- Alam, S., Aubert, M., Avila, S., et al. 2021, *PhRvD*, 103, 083533, doi: [10.1103/PhysRevD.103.083533](https://doi.org/10.1103/PhysRevD.103.083533)
- Amon, A., Blake, C., Heymans, C., et al. 2018, *MNRAS*, 479, 3422, doi: [10.1093/mnras/sty1624](https://doi.org/10.1093/mnras/sty1624)
- Asgari, M., Lin, C.-A., Joachimi, B., et al. 2021, *A&A*, 645, A104, doi: [10.1051/0004-6361/202039070](https://doi.org/10.1051/0004-6361/202039070)
- Baxter, E., Clampitt, J., Giannantonio, T., et al. 2016, *MNRAS*, 461, 4099, doi: [10.1093/mnras/stw1584](https://doi.org/10.1093/mnras/stw1584)
- Baxter, E. J., Omori, Y., Chang, C., et al. 2019, *PhRvD*, 99, 023508, doi: [10.1103/PhysRevD.99.023508](https://doi.org/10.1103/PhysRevD.99.023508)
- Bernstein, G., & Jain, B. 2004, *ApJ*, 600, 17, doi: [10.1086/379768](https://doi.org/10.1086/379768)
- Blake, C., Joudaki, S., Heymans, C., et al. 2016, *MNRAS*, 456, 2806, doi: [10.1093/mnras/stv2875](https://doi.org/10.1093/mnras/stv2875)
- Chisari, N. E., Alonso, D., Krause, E., et al. 2019, *ApJS*, 242, 2, doi: [10.3847/1538-4365/ab1658](https://doi.org/10.3847/1538-4365/ab1658)
- Dark Energy Survey Collaboration, Abbott, T., Abdalla, F. B., et al. 2016, *MNRAS*, 460, 1270, doi: [10.1093/mnras/stw641](https://doi.org/10.1093/mnras/stw641)
- Das, S., & Spergel, D. N. 2009, *PhRvD*, 79, 043509, doi: [10.1103/PhysRevD.79.043509](https://doi.org/10.1103/PhysRevD.79.043509)
- Davis, C., Gatti, M., Vielzeuf, P., et al. 2017, arXiv e-prints, arXiv:1710.02517. <https://arxiv.org/abs/1710.02517>
- de la Torre, S., Jullo, E., Giocoli, C., et al. 2017, *A&A*, 608, A44, doi: [10.1051/0004-6361/201630276](https://doi.org/10.1051/0004-6361/201630276)
- Dey, A., Schlegel, D. J., Lang, D., et al. 2019, *AJ*, 157, 168, doi: [10.3847/1538-3881/ab089d](https://doi.org/10.3847/1538-3881/ab089d)
- Dong, F., Zhang, P., Sun, Z., & Park, C. 2022, *ApJ*, 938, 72, doi: [10.3847/1538-4357/ac905b](https://doi.org/10.3847/1538-4357/ac905b)
- Dong, F., Zhang, P., Zhang, L., et al. 2021, *ApJ*, 923, 153, doi: [10.3847/1538-4357/ac2d31](https://doi.org/10.3847/1538-4357/ac2d31)
- Farrow, D. J., Sánchez, A. G., Ciardullo, R., et al. 2021, *MNRAS*, 507, 3187, doi: [10.1093/mnras/stab1986](https://doi.org/10.1093/mnras/stab1986)
- Giblin, B., Heymans, C., Asgari, M., et al. 2021, *A&A*, 645, A105, doi: [10.1051/0004-6361/202038850](https://doi.org/10.1051/0004-6361/202038850)
- Gong, Y., Miao, H., Zhang, P., & Chen, X. 2021, *ApJ*, 919, 12, doi: [10.3847/1538-4357/ac1350](https://doi.org/10.3847/1538-4357/ac1350)
- Górski, K. M., Hivon, E., Banday, A. J., et al. 2005, *ApJ*, 622, 759, doi: [10.1086/427976](https://doi.org/10.1086/427976)
- Hamilton, A. J. S. 2000, *MNRAS*, 312, 257, doi: [10.1046/j.1365-8711.2000.03071.x](https://doi.org/10.1046/j.1365-8711.2000.03071.x)
- Heymans, C., Van Waerbeke, L., Miller, L., et al. 2012, *MNRAS*, 427, 146, doi: [10.1111/j.1365-2966.2012.21952.x](https://doi.org/10.1111/j.1365-2966.2012.21952.x)
- Hildebrandt, H., Viola, M., Heymans, C., et al. 2017, *MNRAS*, 465, 1454, doi: [10.1093/mnras/stw2805](https://doi.org/10.1093/mnras/stw2805)
- Hildebrandt, H., Köhlinger, F., van den Busch, J. L., et al. 2020, *A&A*, 633, A69, doi: [10.1051/0004-6361/201834878](https://doi.org/10.1051/0004-6361/201834878)
- Hinshaw, G., Larson, D., Komatsu, E., et al. 2013, *ApJS*, 208, 19, doi: [10.1088/0067-0049/208/2/19](https://doi.org/10.1088/0067-0049/208/2/19)
- Jain, B., & Taylor, A. 2003, *PhRvL*, 91, 141302, doi: [10.1103/PhysRevLett.91.141302](https://doi.org/10.1103/PhysRevLett.91.141302)
- Jarvis, M., Bernstein, G., & Jain, B. 2004, *MNRAS*, 352, 338, doi: [10.1111/j.1365-2966.2004.07926.x](https://doi.org/10.1111/j.1365-2966.2004.07926.x)
- Kitching, T. D., Viola, M., Hildebrandt, H., et al. 2015, arXiv e-prints, arXiv:1512.03627. <https://arxiv.org/abs/1512.03627>
- Komatsu, E., Dunkley, J., Nolta, M. R., et al. 2009, *ApJS*, 180, 330, doi: [10.1088/0067-0049/180/2/330](https://doi.org/10.1088/0067-0049/180/2/330)
- Leonard, C. D., Ferreira, P. G., & Heymans, C. 2015, *JCAP*, 2015, 051, doi: [10.1088/1475-7516/2015/12/051](https://doi.org/10.1088/1475-7516/2015/12/051)
- Limber, D. N. 1953, *ApJ*, 117, 134, doi: [10.1086/145672](https://doi.org/10.1086/145672)
- Mandelbaum, R., Hirata, C. M., Seljak, U., et al. 2005, *MNRAS*, 361, 1287, doi: [10.1111/j.1365-2966.2005.09282.x](https://doi.org/10.1111/j.1365-2966.2005.09282.x)
- Miller, L., Heymans, C., Kitching, T. D., et al. 2013, *MNRAS*, 429, 2858, doi: [10.1093/mnras/sts454](https://doi.org/10.1093/mnras/sts454)
- Miyatake, H., Madhavacheril, M. S., Sehgal, N., et al. 2017, *PhRvL*, 118, 161301, doi: [10.1103/PhysRevLett.118.161301](https://doi.org/10.1103/PhysRevLett.118.161301)
- Omori, Y., Giannantonio, T., Porredon, A., et al. 2019, *PhRvD*, 100, 043501, doi: [10.1103/PhysRevD.100.043501](https://doi.org/10.1103/PhysRevD.100.043501)
- Perez, F., & Granger, B. E. 2007, *Computing in Science Engineering*, 9, 21, doi: [10.1109/MCSE.2007.53](https://doi.org/10.1109/MCSE.2007.53)
- Phriksee, A., Jullo, E., Limousin, M., et al. 2020, *MNRAS*, 491, 1643, doi: [10.1093/mnras/stz3049](https://doi.org/10.1093/mnras/stz3049)
- Planck Collaboration, Aghanim, N., Akrami, Y., et al. 2020a, *A&A*, 641, A6, doi: [10.1051/0004-6361/201833910](https://doi.org/10.1051/0004-6361/201833910)
- . 2020b, *A&A*, 641, A8, doi: [10.1051/0004-6361/201833886](https://doi.org/10.1051/0004-6361/201833886)
- Prat, J., Sánchez, C., Fang, Y., et al. 2018, *PhRvD*, 98, 042005, doi: [10.1103/PhysRevD.98.042005](https://doi.org/10.1103/PhysRevD.98.042005)
- Prat, J., Baxter, E., Shin, T., et al. 2019, *MNRAS*, 487, 1363, doi: [10.1093/mnras/stz1309](https://doi.org/10.1093/mnras/stz1309)
- Pullen, A. R., Alam, S., He, S., & Ho, S. 2016, *MNRAS*, 460, 4098, doi: [10.1093/mnras/stw1249](https://doi.org/10.1093/mnras/stw1249)
- Reyes, R., Mandelbaum, R., Seljak, U., et al. 2010, *Nature*, 464, 256, doi: [10.1038/nature08857](https://doi.org/10.1038/nature08857)
- Sánchez, C., Prat, J., Zacharegkas, G., et al. 2021, arXiv e-prints, arXiv:2105.13542. <https://arxiv.org/abs/2105.13542>
- Singh, S., Alam, S., Mandelbaum, R., et al. 2019, *MNRAS*, 482, 785, doi: [10.1093/mnras/sty2681](https://doi.org/10.1093/mnras/sty2681)
- Skara, F., & Perivolaropoulos, L. 2020, *PhRvD*, 101, 063521, doi: [10.1103/PhysRevD.101.063521](https://doi.org/10.1103/PhysRevD.101.063521)
- Spergel, D. N., Verde, L., Peiris, H. V., et al. 2003, *ApJS*, 148, 175, doi: [10.1086/377226](https://doi.org/10.1086/377226)

- Sun, Z., Yao, J., Dong, F., et al. 2022, MNRAS, doi: [10.1093/mnras/stac138](https://doi.org/10.1093/mnras/stac138)
- Taylor, A. N., Kitching, T. D., Bacon, D. J., & Heavens, A. F. 2007, MNRAS, 374, 1377, doi: [10.1111/j.1365-2966.2006.11257.x](https://doi.org/10.1111/j.1365-2966.2006.11257.x)
- van der Walt, S., Colbert, S. C., & Varoquaux, G. 2011, Computing in Science Engineering, 13, 22, doi: [10.1109/MCSE.2011.37](https://doi.org/10.1109/MCSE.2011.37)
- Yao, J., Shan, H., Zhang, P., Kneib, J.-P., & Jullo, E. 2020, ApJ, 904, 135, doi: [10.3847/1538-4357/abc175](https://doi.org/10.3847/1538-4357/abc175)
- Zhang, J., Hui, L., & Stebbins, A. 2005, ApJ, 635, 806, doi: [10.1086/497676](https://doi.org/10.1086/497676)
- Zhang, P. 2006, ApJ, 647, 55, doi: [10.1086/505297](https://doi.org/10.1086/505297)
- Zhang, P., Liguori, M., Bean, R., & Dodelson, S. 2007, PhRvL, 99, 141302, doi: [10.1103/PhysRevLett.99.141302](https://doi.org/10.1103/PhysRevLett.99.141302)
- Zhang, Y., Pullen, A. R., Alam, S., et al. 2021a, MNRAS, 501, 1013, doi: [10.1093/mnras/staa3672](https://doi.org/10.1093/mnras/staa3672)
- Zhang, Z., Wang, H., Luo, W., et al. 2021b, arXiv e-prints, arXiv:2112.04777. <https://arxiv.org/abs/2112.04777>
- Zou, H., Gao, J., Zhou, X., & Kong, X. 2019, ApJS, 242, 8, doi: [10.3847/1538-4365/ab1847](https://doi.org/10.3847/1538-4365/ab1847)
- Zou, H., Gao, J., Xu, X., et al. 2021, ApJS, 253, 56, doi: [10.3847/1538-4365/abe5b0](https://doi.org/10.3847/1538-4365/abe5b0)
- Zu, Y., Shan, H., Zhang, J., et al. 2021, MNRAS, 505, 5117, doi: [10.1093/mnras/stab1712](https://doi.org/10.1093/mnras/stab1712)